JACS
JOURNAL OF THE AMERICAN CHEMICAL SOCIETY
Article
pubs.acs.org/JACS

Remarkable Pressure Responses of Metal–Organic Frameworks: Proton Transfer and Linker Coiling in Zinc Alkyl Gates

Aurélie U. Ortiz,[†] Anne Boutin,[‡] Kevin J. Gagnon,*[,§] Abraham Clearfield,[∥] and François-Xavier Coudert*[,†]

[†]PSL Research University, Chimie ParisTech – CNRS, Institut de Recherche de Chimie Paris, 75005 Paris, France

[‡]École Normale Supérieure, PSL Research University, Département de Chimie, Sorbonne Universités – UPMC Univ Paris 06, CNRS UMR 8640 PASTEUR, 24, rue Lhomond, 75005 Paris, France

[§]Advanced Light Source, Lawrence Berkeley National Laboratory, 1 Cyclotron Road, Berkeley, California 94720, United States

[∥]Department of Chemistry, Texas A&M University, College Station, Texas 77843, United States

Supporting Information

ABSTRACT: Metal–organic frameworks demonstrate a wide variety of behavior in their response to pressure, which can be classified in a rather limited list of categories, including anomalous elastic behavior (e.g., negative linear compressibility, NLC), transitions between crystalline phases, and amorphization. Very few of these mechanisms involve bond rearrangement. Here, we report two novel piezo-mechanical responses of metal–organic frameworks, observed under moderate pressure in two materials of the zinc alkyl gate (ZAG) family. Both materials exhibit NLC at high pressure, due to a structural transition involving a reversible proton transfer between an included water molecule and the linker's phosphonate group. In addition, the 6-carbon alkyl chain of ZAG-6 exhibits a coiling transition under pressure. These phenomena are revealed by combining high-pressure single-crystal X-ray crystallography and quantum mechanical calculations. They represent novel pressure responses for metal–organic frameworks, and pressure-induced proton transfer is a very rare phenomenon in materials in general.

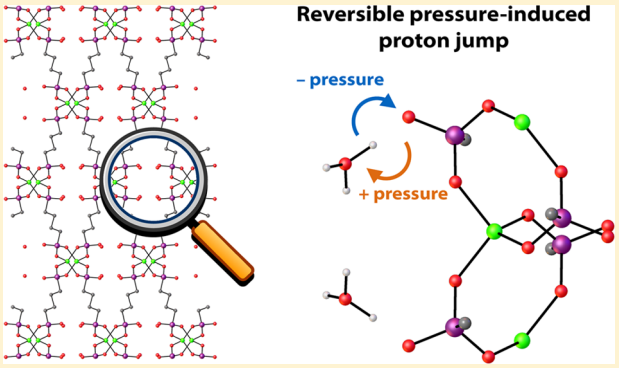

I. INTRODUCTION

Molecular framework materials, and in particular metal–organic frameworks (MOFs), demonstrate a wide variety of behavior in their response to pressure. For small-scale deformations, examples of anomalous elastic mechanical properties include negative linear compressibility (NLC),[1,2] negative area compressibility,[3] and exceptionally low[4] and extremely anisotropic[5] elastic moduli. Larger-scale deformations, in the form of pressure-induced phase transformations, are another possible response to mechanical stimulation and have been widely explored in metal–organic frameworks, with a gamut of phenomena that include pressure-induced amorphization,[6] "gate opening" in interpenetrated or stacked-layer frameworks,[7,8] and "breathing" transitions[9] in frameworks with a wine rack geometric motif.[10] The number of reported materials (sometimes called *soft porous crystals*[11]) showing pressure-induced, temperature-induced, or adsorption-induced phase transformations has been steadily increasing through the past decade. Entire reviews[12,13] have been devoted to the subject, and although none of these materials have yet been directly used at the industrial scale,[14] they have been proposed for a variety of practical applications,[12] such as sensing traces of organic molecules,[13] slow release of drugs for long-release single-injection therapies,[15] and specific gas separations.[16,17]

Despite the fast-increasing number of MOFs exhibiting pressure-induced phase transformations, most of these materials share some common characteristics. First, the vast majority of transitions reported experimentally do not involve bond breaking, bond formation, or bond rearrangement. Pressure-induced bond rearrangement, and in particular *reversible* pressure-induced bond rearrangement, is a very rare phenomenon in materials science. Two exceptional examples are the molecular framework $Ag_3[Co(CN)_6]$[18] and a recently reported erbium–formate metal–organic framework.[19] Second, the structures of most soft porous crystals can be decomposed as a combination of underlying mechanical building units. The most common root of large-scale flexibility then arises from the combination of some of these mechanical building units acting as hinges and others acting as rigid struts.[20] This separation of the degrees of freedoms allows flexible molecular frameworks to present very soft deformation modes involving the hinges,[21] while retaining crystalline characteristics and lattice integrity

Received: June 18, 2014
Published: July 18, 2014

   dx.doi.org/10.1021/ja5060059 | J. Am. Chem. Soc. 2014, 136, 11540–11545

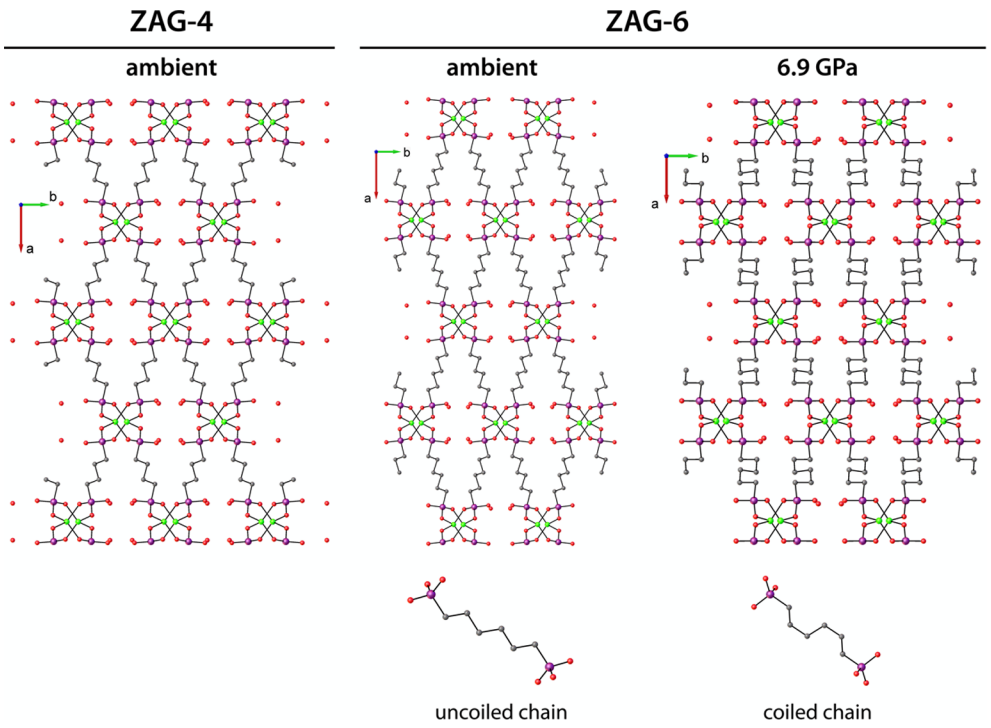

Figure 1. ZAG-4 structure at ambient conditions (left) and ZAG-6 structures at ambient conditions (center) and 6.9 GPa (right), viewed along the *c* axis, showing the wine rack framework (Zn: green; P: purple; C: black; H: white; O: red). The bottom panels show the conformation adopted by the 1,6-hexanebisphosphonate chain of ZAG-6: noncoiled at ambient conditions, coiled at higher pressure.

due to the stiffness of the struts. Investigations into flexible materials combining hinges joined by flexible organic linkers have only just started to appear and showed that the extra flexibility of the linker does really increase the complexity of the system and the richness of its behavior under mechanical[22] or adsorptive stimulation.[23] For example, a study of CAU-13 demonstrated that xylene adsorption induces a breathing transition of its wine rack framework, along with a change of conformation of half its 1,4-cyclohexanedicarboxylate linkers from *a*,*a* to *e*,*e*.[23]

Here, we report a study of the behavior under pressure of two zinc alkyl gate (ZAG) materials,[24−26] a family of metal−organic frameworks that present a common wine rack geometric motif but use alkyl chains as the linker molecules, by combining in situ single-crystal X-ray diffraction at high pressure and quantum chemical calculations. We show that both materials, ZAG-4 and ZAG-6, exhibit negative linear compressibility at high pressure and demonstrate that this NLC is due to the occurrence of a pressure-induced structural transition involving a reversible proton transfer between an included water molecule and the linker's phosphonate group. Moreover, while the 4-carbon alkyl chain of ZAG-4 acts as a rigid linker, we show that the 6-carbon alkyl chain of ZAG-6 exhibits a coiling transition under pressure, and we provide molecular insight into the driving force of this transition. Both pressure-induced transitions (proton jump and linker coiling) are novel as pressure responses for a metal−organic framework. In addition, the occurrence of a pressure-induced proton transfer is a very rare phenomenon and the first case ever reported for a metal−organic framework.

II. RESULTS AND DISCUSSION

Two isoreticular compounds, ZAG-4 and ZAG-6, share the same connectivity but differ through length of the alkyl linker, either 4 or 6 carbon atoms in length. The ZAG compounds are comprised of Zn−O−P−O eight-membered rings which are corner fused through the zinc atoms to form a 1-D chain along the *c*-axis. These chains are bridged in one direction via the alkyl spacers and are hydrogen bonded to neighboring chains in the other direction. The nature of this hydrogen bond connection is through the use of interstitial water molecules which each form three hydrogen bonds, two to the framework and one from the framework.

1. Origin of Negative Linear Compressibility in ZAG-4.

The behavior of ZAG-4 under pressure, which has been reported experimentally,[25] presents two characteristic features: a nonmonotonic evolution of unit cell parameters and the presence of negative linear compressibility at pressure higher than 2 GPa. To explain these uncharacteristic features, we performed quantum mechanical calculations of the relaxed structure of ZAG-4 and its mechanical properties in the elastic regime. The calculated optimized structure gives a good agreement with the experimental crystallographic data at ambient conditions (see Table S1, Supporting Information). Moreover, we were able to confirm through this calculation the exact position of the hydrogen atoms, which could not be refined from the single-crystal X-ray diffraction experiments. In particular, this allows us to confirm the unprotonated state of the included water molecule, forming three hydrogen bonds with the framework: donating two H bonds to two distinct neighboring phosphonate groups (calculated HOH···O′ distances of 1.79 and 1.83 Å; O···O′ distances of 2.77 and 2.81 Å) as well as accepting one very strong H bond from third phosphonate group on the opposite side of the wine rack motif (calculated POH···OH_2 distance of 1.46 Å; O···O′ distance of 2.50 Å).

Because the ZAG-4 framework shows a wine rack motif in the plane perpendicular to *c* (see Figure 1) and wine rack

dx.doi.org/10.1021/ja5060059 | J. Am. Chem. Soc. 2014, 136, 11540−11545

frameworks typically exhibit NLC,[20,21] we first look at the directional dependence of the linear compressibility (LC) in the elastic regime, as derived from the elastic stiffness matrix (Table S2, Supporting Information). The high anisotropy of

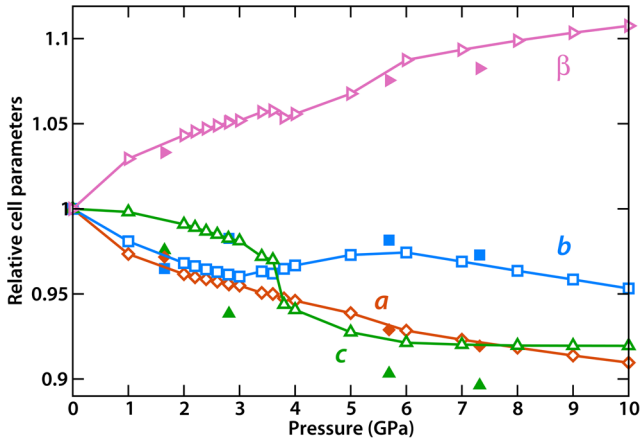

Figure 2. Evolution of the unit cell parameters of ZAG-4 as a function of pressure. Filled symbols: from in situ X-ray diffraction. Empty symbols: calculated by quantum mechanical enthalpy minimization.

the elastic moduli (Young's and shear moduli, Table S3, Supporting Information) shows that ZAG-4 presents some of the characteristics of soft porous crystals, while being overall more robust (bulk modulus of 15.7 GPa, compared to 2−5 GPa for soft porous crystals) due to its denser structure: it thus ranks somewhere between *rigid* and *breathing* metal−organic frameworks. Likewise, ZAG-4 exhibits a single direction of NLC, along the longer axis of the wine rack (the LC is shown as a 3D surface in Figure S1, Supporting Information). However, the value of the NLC (-18 TPa^{-1}) is modest compared to porous wine rack frameworks. Moreover, this elastic NLC cannot account for the experimental observation of NLC at higher pressure, which is primarily along a different direction (the *b* crystallographic axis). In fact, our calculations predict a positive LC for the *b* axis (β_b = +29 TPa^{-1}) in the elastic regime.

We thus performed an in silico experiment of compression of the ZAG-4 framework, by a series of enthalpy minimization calculations at increasing values of pressure. This methodology can help understand deformation outside the elastic regime and predict structural transitions, as recently shown in the case of metal−organic frameworks CAU-13 and NOTT-300.[22] The evolution of unit cell parameters as a function of pressure, shown in Figure 2, is in good agreement with the experimental data: it clearly confirms the nonmonotonic evolution of the *b* parameter and shows that its change in slope is linked to a sudden decrease of *c* (which was not visible on the experimental data due to the small number of pressure points measured). The negative linear compressibility of ZAG-4 above 2 GPa is in fact due to the occurrence of a structural transition happening at 3.8 GPa.

2. Pressure-Induced Proton Transfer. Looking at the minimal-enthalpy structures calculated before and after the transition (for 3.6 and 3.8 GPa), we see that it is associated with the transfer of a proton from the framework's phosphonate group to the included water molecule (see Figure S2, Supporting Information, for a visualization of the geometry of the protonated state)

$$R{-}PO_3H + H_2O \rightarrow R{-}PO_3^- + H_3O^+$$

Given that the right-hand side of this chemical equation features two ionic species, we need to better understand why pressure stabilizes their coexistence in close vicinity. The answer, and the driving force of this proton transfer, can be found in the evolution of O−H distances (Figure 3) between the proton and the oxygen atoms of the water and phosphonate group, obtained from quantum chemical calculations: the compression of the material's main effect is to bring the $-PO_3H$ group closer to the water molecule, as the wine rack pore is compressed. Then, the jump of the proton allows us to form the very short 1.05 Å O−H bond in H_3O^+, which yields an overall smaller distance of the two oxygen atoms (2.4 Å after the jump vs 2.5 Å before the jump). The formation of the ionic species allows for a shorter O−O distance overall and thus a smaller unit cell volume, which is a favorable process when the pressure is enough to overcome the initial energy penalty ($P\Delta V > \Delta E$).

To shed more light onto the properties of this pressure-induced proton transfer, a piezo-mechanical response never reported before for a metal−organic framework, we performed

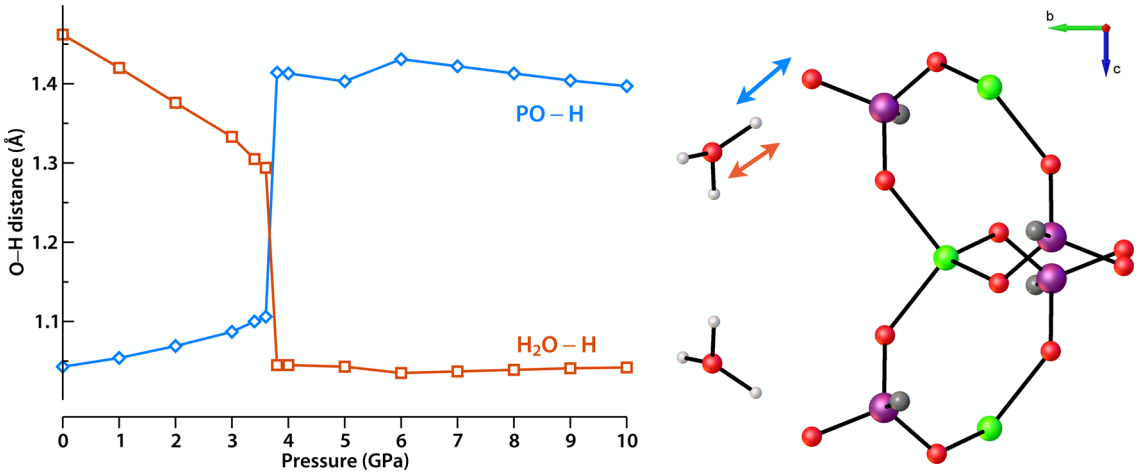

Figure 3. Evolution of the distance of the hopping proton from the oxygen in $R{-}PO_3H$ and H_2O, as pressure increases. On the right are represented the protonated water molecule and local framework environment, with the two distances indicated by arrows.

dx.doi.org/10.1021/ja5060059 | J. Am. Chem. Soc. 2014, 136, 11540−11545

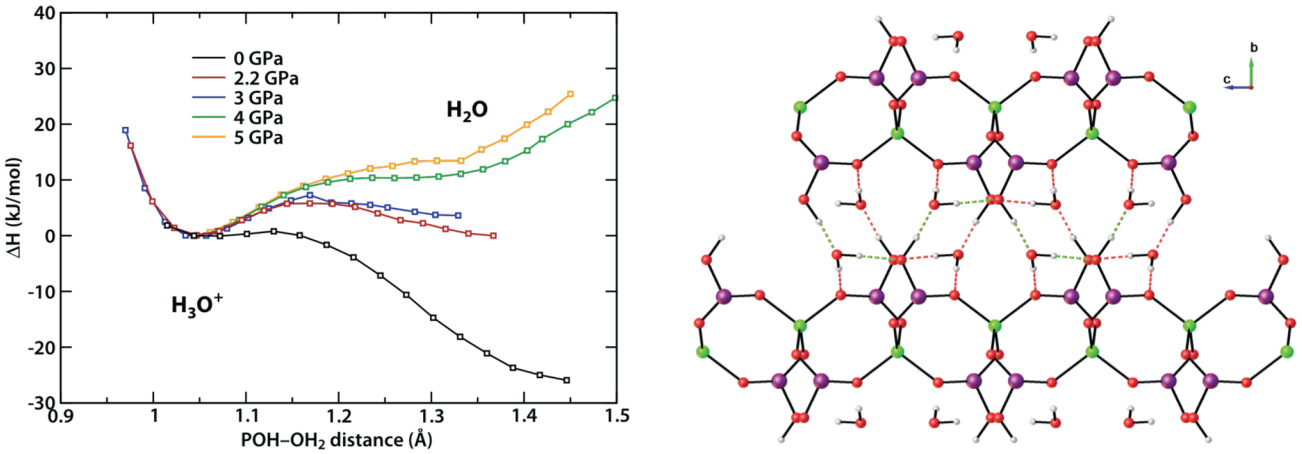

Figure 4. Left: Enthalpy profiles for the proton jump in ZAG-4, scanned along the proton–water distance, at various values of pressure. Enthalpy is reported in units of kJ/mol per primitive cell (which contains 4 H_2O). Right: Representation of the 1D chains of hydrogen bonds in ZAG-4, along which the proton can diffuse at intermediate pressure (~2 GPa) in a Grotthuss-like mechanism.

calculations of the enthalpy profile of the proton transfer at various values of pressure (shown in Figure 4). First, we confirm that the proton is well localized on the phosphonate group at ambient conditions, with a stabilization energy of 26 kJ/mol (per primitive cell, i.e., 52 kJ/mol per unit cell or 6.5 kJ/mol per water molecule) in favor of the neutral state, and on the water molecule at high pressure, with a stabilization of 14 kJ/mol at 5 GPa. We thus truly have a proton transfer from one state to another and not a delocalized state. The equilibrium pressure for the two states, at which the enthalpy is equal, is 2.2 GPa.

Moreover, we see that the enthalpy barrier at intermediate pressures becomes quite low, down to 6 kJ/mol at 2.2 GPa (which corresponds to 2.4kT at room temperature). The proton can thus be expected to diffuse fast along the one-dimensional network of hydrogen-bonded water and phosphonate groups, along the c axis (Figure 4, right), via a Grottthuss mechanism. We propose that ZAG-4 is thus a good candidate for a pressure-switchable proton conduction material. This property, shown recently on brucite at 11 GPa by single-crystal experiments,[27] is useful for applications as nanodevices, sensors, or actuators. In the case of ZAG-4, the relative softness of the metal–organic framework (compared to dense inorganic materials such as brucite) has the extra advantage that the effect is observed at much lower pressure.

3. Effect of Linker Chain Length: Pressure-Induced Linker Coiling in ZAG-6. To study the effect of the linker's alkyl chain length on the flexibility of ZAG materials, we performed single-crystal X-ray diffraction experiments on ZAG-6 at ambient pressure and high pressure (P = 6.9 GPa). The crystallographic structures obtained are available as Supporting Information, and their unit cell parameters are summarized in Table S4 (Supporting Information). At ambient conditions, ZAG-6 presents the same "wine rack" geometry (Figure 1, left) as ZAG-4, and its pores also contain one water molecule in close proximity of each phosphonate group (eight of each per unit cell). At high pressure (P = 6.9 GPa), we observe again a negative linear compressibility along the b axis (2% expansion), due to the compression of the wine rack motif. However, the high-pressure structure of ZAG-6 is geometrically different than its ambient pressure structure, in the form of a coiling of the hexanediphosphonate chain. This piezo-mechanical response, depicted in Figure 1 (bottom), is not observed in ZAG-4 due to its shorter butanediphosphonate linker: the P–C–C–C and C–C–C–C dihedral angles in ZAG-4 stay equal to 180° at all pressures investigated, while in ZAG-6 at 6.9 GPa they distort from 177.1(2)° to 170.2(6)° (for P–C_1–C_2–C_3) and from 173.7(3)° to 55.3(10)° (for C_1–C_2–C_3–C_4).

This pressure-induced coiling of a flexible linker chain is a novel piezo-mechanical behavior in flexible MOFs, which has never been demonstrated before. To investigate it further, and to determine if ZAG-6 also presents a pressure-induced proton jump, we performed quantum chemical calculations. We considered four possible "states" of the ZAG-6 structure: with either straight or coiled alkyl chain (denoted *straight* and *coiled*) and with the proton either on the phosphonate group or the water molecule (denoted H_2O and H_3O^+, respectively). Each of the structures turns out to be metastable (i.e., a local energy minimum), and we studied their enthalpy as a function of pressure, reported in Figure 5 with the *straight*–H_2O structure taken as a reference.[28]

First, we confirm that the *straight*–H_2O conformation (with a straight alkyl chain and unprotonated water molecule) is the most stable in ambient conditions: the energetic cost of coiling the ZAG-6 chain is 15 kJ/mol per primitive cell (i.e., 7.5 kJ/

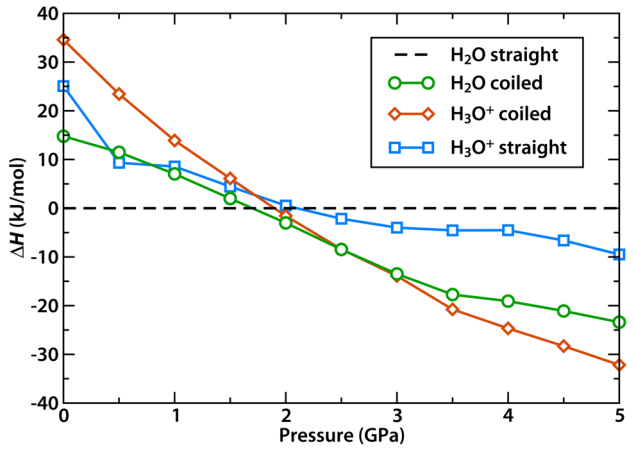

Figure 5. Relative enthalpies of the four possible metastable phases of ZAG-6 as a function of pressure. The enthalpy reference is taken to be the ambient phase, i.e., the uncoiled H_2O structure. The units are kJ/mol per primitive cell.

dx.doi.org/10.1021/ja5060059 | J. Am. Chem. Soc. 2014, 136, 11540–11545

mol, or ~3 *kT*, per alkyl chain), while the charge transfer state $\{R-PO_3^-, H_3O^+\}$ is destabilized by 25 kJ/mol (which is the same energy difference as in ZAG-4). Second, as we increase pressure, the enthalpy of the H_3O^+ and *coiled* structures becomes smaller compared to the "ambient" *straight*−H_2O conformation. This is because both have a smaller unit cell volume than *straight*−H_2O: coiling the chain reduces its length, and transferring the proton to the water molecules means that the phosphonate−water distance can be reduced overall (as already shown for ZAG-4). Therefore, at pressures higher than 3 GPa, we predict that the *coiled*−H_3O^+ is the most stable structure, with both factors minimizing the *PV* contribution to the enthalpy. This confirms the experimentally observed coiling and its driving force, as well as the occurrence of a pressure-induced proton jump in ZAG-6, similar to that in ZAG-4. Moreover, the very close enthalpies for the *coiled*−H_2O and *coiled*−H_3O^+ structures in the intermediate range of pressure (2−3 GPa) indicate that the proton is fairly delocalized at these pressures. This makes ZAG-6, like ZAG-4, a good candidate pressure-switchable proton conduction material. Finally, in addition to the above theoretical evidence for the proton hop in the ZAG-6 compound, we also experimentally see a shortening of the P−O bond distance from 1.562(2) to 1.503(9) Å, which is indicative of the change of the phosphonic acid to a phosphonate and indirect experimental evidence of the pressure-induced proton jump. A future neutron diffraction study on deuterated compounds should provide a direct experimental confirmation.

III. CONCLUSION

Herein we report two novel piezo-mechanical responses of MOFs, identified in the behavior of the ZAG family under moderate pressure. Both materials undergo a unique bond rearrangement involving a protonated phosphonic acid group and an interstitial water molecule, explaining the nonlinear evolution of cell parameters under pressure. Furthermore, the ZAG-6 compound undergoes a unique chain-coiling mechanism in response to added pressure. Both of these piezo-mechanical responses are rare phenomena under pressure and are herein reported for the first time in a MOF material. In addition to these unique piezo-mechanical responses, both materials also exhibit negative linear compressibility. The combination of these three responses to external pressure present in a small family of MOF type materials helps to establish just how deep the field of MOFs may be with future study into mechanical properties. These types of materials may yet provide new insight into crystal physics and properties, as well as practical applications as pressure-switchable proton conduction materials. These properties will be studied in future work by in situ electrochemical impedance spectroscopy under hydrostatic pressure.

IV. METHODS

1. Experimental Section. The pressure-dependent studies of ZAG-6 were conducted on a single-crystal sample of dimensions 120 × 80 × 40 μm. The sample was loaded into a Merrill-Bassett-type diamond anvil cell (DAC) with Bohler-Almax cut diamonds, with culets of 600 μm in tungsten-carbide backing seats and a tungsten gasket with hole diameter of 350 μm. The pressure medium used was a 4:1 methanol/ethanol mixture. The crystal was first affixed to the surface of the diamond culet using a silicon vacuum grease before the gasket was set in place. A small amount of ruby powder was added for pressure calibration and the methanol/ethanol added before closing the DAC. The cell was pressurized to 6.9(4) GPa initially and was allowed to stabilize for 3 h before data collection.

Data collection was performed at Beamline 11.3.1 at the Advanced Light Source (ALS) at Lawrence Berkeley National Lab (LBNL). In situ diffraction experiments were performed using silicon (111) monochromated synchrotron radiation (λ = 0.6702 Å) on a modified Bruker APEX-II diffractometer system. The ambient diffraction data were collected on the same Bruker APEX-II diffractometer using synchrotron radiation (λ = 0.6048 Å). The pressure of the cell was monitored via ruby fluorescence stimulated by a 100 W 447 nm diode, measured via fiber-optic coupled to a Princeton Instruments Acton 300i spectrometer. The ambient data were collected on a single crystal mounted on a MiTeGen kapton pin at room temperature. The structures were solved by intrinsic phasing methods (SHELXT) and refined by full-matrix least-squares on F^2 (SHELXL-2014). All non-hydrogen atoms were refined anisotropically. Hydrogen atoms were geometrically calculated and refined as riding atoms. The hydrogen atoms on the hydroxyl and water oxygen atoms were found in the difference map, their distances restrained (0.85 Å) and refined with a riding model. Additional crystallographic information has been summarized in Table S4 (Supporting Information) and full details can be found in the crystallographic information files provided in the Supporting Information.

2. Quantum Chemical Calculations. The mechanical properties of ZAG-4 and ZAG-6 were calculated on a first-principles basis by a two-stage methodology relying on quantum chemical calculations. First, we characterized the elastic properties of the structures using calculations in the density functional theory approach with localized basis sets (CRYSTAL09 code[29]) and the B3LYP hybrid exchange−correlation functional,[30] with all electron basis sets for all atoms involved: 6-311G(d,p) for H, C, and O,[31] 85-21d1G for P,[32] and 86-411d31G for Zn.[33] This state-of-the-art methodology has been well validated on both rigid[4] and flexible MOFs.[5,22] From the full stiffness matrices of ZAG-4 and ZAG-6, containing 13 independent second-order elastic constants due to their monoclinic nature, tensorial analysis[21] allowed us to extract from these the directional Young's modulus, shear modulus, linear compressibility, and Poisson's ratio in the elastic regime.

In addition, to study the piezo-mechanical behavior of the ZAG materials outside of the linear elastic domain, we performed in silico compression experiments by enthalpy minimization as a function of varying pressure. For each value of isotropic pressure applied, the materials (ZAG-4 and ZAG-6) were fully relaxed (enthalpy minimized) by optimizing both atomic positions and unit cell parameters, with full use of the crystals' symmetry (space group *C*2/*c*, consistent with the experimental structures at both ambient and high pressure). The structures obtained were all checked for possible higher symmetry, but none was found. For ZAG-4, we started from the experimental ambient structure and observed a spontaneous proton jump at P = 3.8 GPa.

For ZAG-6, neither the proton jump nor the alkyl chain twisting occurred spontaneously during the in silico compression starting from the experimental ambient structure. We attribute this difference to the larger dimensionality of the configuration space of the material and the metastability of this state. Thus, to study the proton jump and linker coiling transitions, we performed four separate series of pressure calculations starting from the metastable H_2O/H_3O^+ and *straight*/*coiled* conformations (see section 3) and fully relaxing them at varying pressure (enthalpy minimization). We found that, in the 0−5 GPa range of pressure, all four conformations were indeed metastable and plotted their enthalpy as a function of pressure.

Finally, we performed a calculation of the enthalpy profiles for the proton jump in ZAG-4, at various values of external pressure. For each pressure, we performed constrained enthalpy minimization at a series of fixed proton−water distance. While this distance was kept constrained, the rest of the system (atomic positions and unit cell parameters) was fully relaxed.

dx.doi.org/10.1021/ja5060059 | J. Am. Chem. Soc. 2014, 136, 11540−11545

■ ASSOCIATED CONTENT

Supporting Information

Experimental and computational crystallographic structures, elastic matrices and mechanical properties, and additional figures. This material is available free of charge via the Internet at http://pubs.acs.org.

■ AUTHOR INFORMATION

Corresponding Authors

kjgagnon@lbl.gov
fx.coudert@chimie-paristech.fr

Notes

The authors declare no competing financial interest.

■ ACKNOWLEDGMENTS

We thank Rodolphe Vuilleumier and Alain Fuchs for fruitful discussions. We acknowledge funding from Agence Nationale de la Recherche (project ANR-2010-BLAN-0822), the National Science Foundation (grant DMR-0652166), as well as the Robert A. Welch Foundation (grant A-0673) and computing time on HPC platforms by GENCI (grants i2014086114 and i2014087069). K.J.G. thanks the National Science Foundation for support through the NSF GRFP grant no. DGE-0750732. The Advanced Light Source is supported by the Director, Office of Science, Office of Basic Energy Sciences, of the U.S. Department of Energy under Contract No. DEAC02-05CH11231.

■ REFERENCES

(1) Cairns, A. B.; Catafesta, J.; Levelut, C.; Rouquette, J.; van der Lee, A.; Peters, L.; Thompson, A. L.; Dmitriev, V.; Haines, J.; Goodwin, A. L. *Nat. Mater.* **2013**, *12*, 212−216.

(2) Li, W.; Probert, M. R.; Kosa, M.; Bennett, T. D.; Thirumurugan, A.; Burwood, R. P.; Parinello, M.; Howard, J. A. K.; Cheetham, A. K. *J. Am. Chem. Soc.* **2012**, *134*, 11940−11943.

(3) Hodgson, S. A.; Adamson, J.; Hunt, S. J.; Cliffe, M. J.; Cairns, A. B.; Thompson, A. L.; Tucker, M. G.; Funnell, N. P.; Goodwin, A. L. *Chem. Commun.* **2014**, *50*, 5264−5266.

(4) Tan, J. C.; Civalleri, B.; Lin, C.-C.; Valenzano, L.; Galvelis, R.; Chen, P.-F.; Bennett, T.; Mellot-Draznieks, C.; Zicovich-Wilson, C.; Cheetham, A. *Phys. Rev. Lett.* **2012**, *108*, 095502.

(5) Ortiz, A.; Boutin, A.; Fuchs, A.; Coudert, F.-X. *Phys. Rev. Lett.* **2012**, *109*, 195502.

(6) Chapman, K. W.; Halder, G. J.; Chupas, P. J. *J. Am. Chem. Soc.* **2009**, *131*, 17546−17547.

(7) Kitaura, R.; Seki, K.; Akiyama, G.; Kitagawa, S. *Angew. Chem., Int. Ed.* **2003**, *42*, 428−431.

(8) Tanaka, D.; Nakagawa, K.; Higuchi, M.; Horike, S.; Kubota, Y.; Kobayashi, T. C.; Takata, M.; Kitagawa, S. *Angew. Chem., Int. Ed.* **2008**, *47*, 3914−3918.

(9) Serre, C.; Bourrelly, S.; Vimont, A.; Ramsahye, N. A.; Maurin, G.; Llewellyn, P. L.; Daturi, M.; Filinchuk, Y.; Leynaud, O.; Barnes, P.; Férey, G. *Adv. Mater.* **2007**, *19*, 2246−2251.

(10) Coudert, F.-X.; Boutin, A.; Fuchs, A. H.; Neimark, A. V. *J. Phys. Chem. Lett.* **2013**, *4*, 3198−3205.

(11) Horike, S.; Shimomura, S.; Kitagawa, S. *Nat. Chem.* **2009**, *1*, 695−704.

(12) Bureekaew, S.; Shimomura, S.; Kitagawa, S. *Sci. Technol. Adv. Mater.* **2008**, *9*, 014108.

(13) Férey, G.; Serre, C. *Chem. Soc. Rev.* **2009**, *38*, 1380−1399.

(14) Czaja, A. U.; Trukhan, N.; Mueller, U. *Chem. Soc. Rev.* **2009**, *38*, 1284−1293.

(15) Horcajada, P.; Serre, C.; Maurin, G.; Ramsahye, N. A.; Balas, F.; Vallet-Regi, M.; Sebban, M.; Taulelle, F.; Férey, G. *J. Am. Chem. Soc.* **2008**, *130*, 6774−6780.

(16) Thallapally, P. K.; Tian, J.; Kishan, M. R.; Fernandez, C. A.; Dalgamo, S. J.; McGrail, P. B.; Warren, J. E.; Atwood, J. L. *J. Am. Chem. Soc.* **2008**, *130*, 16842−16843.

(17) Remy, T.; Baron, G. V.; Denayer, J. F. M. *Langmuir* **2011**, *27*, 13064−13071.

(18) Goodwin, A. L.; Keen, D. A.; Tucker, M. G. *Proc. Nat. Acad. Sci.* **2008**, *105*, 18708−18713.

(19) Spencer, E. C.; Kiran, M. S. R. N.; Li, W.; Ramamurty, U.; Ross, N. L.; Cheetham, A. K. *Angew. Chem., Int. Ed.* **2014**, *53*, 5583−5586.

(20) Ogborn, J. M.; Collings, I. E.; Moggach, S. A.; Thompson, A. L.; Goodwin, A. L. *Chem. Sci.* **2012**, *3*, 3011−3017.

(21) Ortiz, A. U.; Boutin, A.; Fuchs, A. H.; Coudert, F.-X. *J. Chem. Phys.* **2013**, *138*, 174703.

(22) Ortiz, A.; Boutin, A.; Coudert, F.-X. *Chem. Commun.* **2014**, *50*, 5867−5870.

(23) Niekiel, F.; Lannoeye, J.; Reinsch, H.; Munn, A. S.; Heerwig, A.; Zizak, I.; Kaskel, S.; Walton, R. I.; de Vos, D.; Llewellyn, P.; Lieb, A.; Maurin, G.; Stock, N. *Inorg. Chem.* **2014**, *53*, 4610−4620.

(24) Gagnon, K. J.; Perry, H. P.; Clearfield, A. *Chem. Rev.* **2012**, *112*, 1034−1054.

(25) Gagnon, K. J.; Beavers, C. M.; Clearfield, A. *J. Am. Chem. Soc.* **2013**, *135*, 1252−1255.

(26) Gagnon, K. J.; Teat, S. J.; Beal, Z. J.; Embry, A. M.; Strayer, M. E.; Clearfield, A. *Cryst. Growth Des.* **2014**, *14*, 3612−3622.

(27) Guo, X.; Yoshino, T. *Geophys. Res. Lett.* **2014**, *41*, 813−819.

(28) It should be noted that, while at finite temperature the transition will be dictated by the relative Gibbs free energy of the phases, $G = H - TS$, in our quantum chemical calculations we are restricted to the calculations of the enthalpy, H. The entropic effects are thus, in this approach, neglected.

(29) Dovesi, R.; Orlando, R.; Civalleri, B.; Roetti, C.; Saunders, V. R.; Zicovich-Wilson, C. M. *Z. Kristallogr.* **2005**, *220*, 571.

(30) Becke, A. D. *J. Chem. Phys.* **1993**, *98*, 5648.

(31) Catti, M.; Valerio, G.; Dovesi, R.; Causa, M. *Phys. Rev. B* **1994**, *49*, 14179−14187.

(32) Corno, M.; Busco, C.; Civalleri, B.; Ugliengo, P. *Phys. Chem. Chem. Phys.* **2006**, *8*, 2464−2472.

(33) Jaffe, J. E.; Hess, A. C. *Phys. Rev. B* **1993**, *48*, 7903.